Virus-helminth coinfection reveals a microbiota-independent mechanism of immunomodulation

Lisa C. Osborne *et al.*

Science **345**, 578 (2014);
DOI: 10.1126/science.1256942

COINFECTION

Virus-helminth coinfection reveals a microbiota-independent mechanism of immunomodulation

Lisa C. Osborne,[1,2] Laurel A. Monticelli,[1,2] Timothy J. Nice,[3] Tara E. Sutherland,[4] Mark C. Siracusa,[1,2]* Matthew R. Hepworth,[1,2,5] Vesselin T. Tomov,[5] Dmytro Kobuley,[1,2] Sara V. Tran,[1,2] Kyle Bittinger,[1] Aubrey G. Bailey,[1] Alice L. Laughlin,[1] Jean-Luc Boucher,[6] E. John Wherry,[2] Frederic D. Bushman,[1] Judith E. Allen,[4] Herbert W. Virgin,[3] David Artis[1,2,7]†

The mammalian intestine is colonized by beneficial commensal bacteria and is a site of infection by pathogens, including helminth parasites. Helminths induce potent immunomodulatory effects, but whether these effects are mediated by direct regulation of host immunity or indirectly through eliciting changes in the microbiota is unknown. We tested this in the context of virus-helminth coinfection. Helminth coinfection resulted in impaired antiviral immunity and was associated with changes in the microbiota and STAT6-dependent helminth-induced alternative activation of macrophages. Notably, helminth-induced impairment of antiviral immunity was evident in germ-free mice, but neutralization of Ym1, a chitinase-like molecule that is associated with alternatively activated macrophages, could partially restore antiviral immunity. These data indicate that helminth-induced immunomodulation occurs independently of changes in the microbiota but is dependent on Ym1.

The microbiota of the mammalian gastrointestinal (GI) tract is composed of trillions of beneficial commensal bacteria that promote nutrient metabolism and regulate multiple physiological processes (*1*, *2*). The GI tract is also a common site of infection by pathogenic viruses, bacteria, protozoa, and helminths. The dynamic cross-regulation that exists between the host, the microbiota, and enteric pathogens regulates intestinal homeostasis (*3*–*9*), indicating that these are highly coevolved relationships. Signals derived from commensal bacteria and helminth parasites can influence the mammalian immune response (*1*, *2*, *10*–*12*), and helminth infection can elicit alterations in the composition of commensal bacteria that have been associated with limiting inflammation in multiple tissues (*13*–*16*). Despite speculation regarding whether helminth-induced immunomodulation is mediated through direct effects on the mammalian immune system or indirectly via changes in the microbiota (*14*, *17*, *18*), this fundamental question has not been addressed. Given the impact of helminth-elicited immunomodulation both as a risk factor for bacterial, viral, and protozoan coinfection (*19*–*22*) and as a potential therapeutic strategy for multiple inflammatory diseases including asthma, multiple sclerosis, and inflammatory bowel disease (*23*, *24*),

[1]Department of Microbiology, Perelman School of Medicine, University of Pennsylvania, Philadelphia, PA 19104, USA. [2]Institute for Immunology, Perelman School of Medicine, University of Pennsylvania, Philadelphia, PA 19104, USA. [3]Department of Pathology and Immunology, Washington University School of Medicine, St. Louis, MO 63110, USA. [4]Institute of Immunology and Infection Research, Centre for Immunity, Infection and Evolution, School of Biological Sciences, University of Edinburgh, Edinburgh EH9 3JT, UK. [5]Department of Medicine, Division of Gastroenterology, Perelman School of Medicine, University of Pennsylvania, Philadelphia, PA 19104, USA. [6]Laboratoire de Chimie et Biochimie Pharmacologiques et Toxicologiques, Université Paris Descartes, Paris, France. [7]Department of Pathobiology, School of Veterinary Medicine, University of Pennsylvania, Philadelphia, PA 19104, USA. *Present address: Department of Medicine, Rutgers New Jersey Medical School, Newark, NJ 07103, USA. †Corresponding author. E-mail: dartis@mail.med.upenn.edu

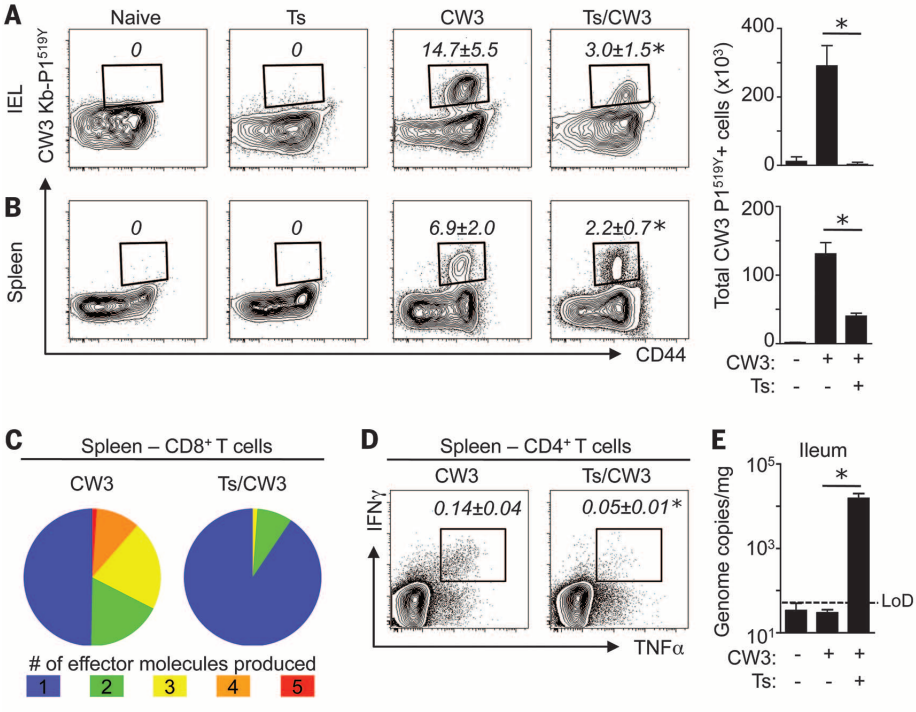

Fig. 1. Helminth coinfection impairs immunity to enteric viral infection. C57BL/6 mice were either left naïve or infected with 500 *Trichinella spiralis* (Ts) larvae per os (po). At day 12 post-*Trichinella* infection, mice were infected with 10^6 plaque-forming units (pfu) MNV CW3 (po) and killed at day 8 post-CW3 infection. (**A** and **B**) Flow cytometric detection of antigen-specific MNV CW3 $P1^{519Y}$ tetramer$^+$ CD8$^+$ T cells in naïve, *Trichinella* (Ts)–infected, CW3-infected, or Ts/CW3–coinfected mice in the (A) small intestine intraepithelial lymphocytes (IEL) and (B) spleen. Numbers in flow plots represent mean frequencies ± SEM of CW3 Kb-$P1^{519Y}$ tetramer$^+$ cells within the CD8$^+$ lymphocyte gate of each group. Error bars in bar graphs indicate SEM. (**C**) Splenocytes from CW3 and Ts/CW3 mice were stimulated with MNV CW3 $P1^{519Y}$ peptide and assayed for production of IFN-γ, TNF-α, chemokine (C-C motif) ligand 3, CD107a, and granzyme B. Pie charts show fractions of peptide-responsive CD8$^+$ T cells producing any combination of these effector molecules. (**D**) Splenocytes from mono- and coinfected mice were stimulated with a pool of MHCII IA^b–restricted MNV-specific peptides and assayed for production of IFN-γ and TNF-α. Numbers in flow plots represent mean frequencies ± SEM of dual-producing IFN-γ$^+$ TNF-α$^+$ cells within the CD4$^+$ CD44^{hi} lymphocyte gate of each group. (**E**) MNV genome copies in ileal tissue were quantified by real-time polymerase chain reaction (RT-PCR). All data are representative of two to four independent experiments with a minimum of three to five mice per group. Statistics compared monoinfected versus coinfected groups by using the Student's *t* test. *$P < 0.05$. LoD, limit of detection.

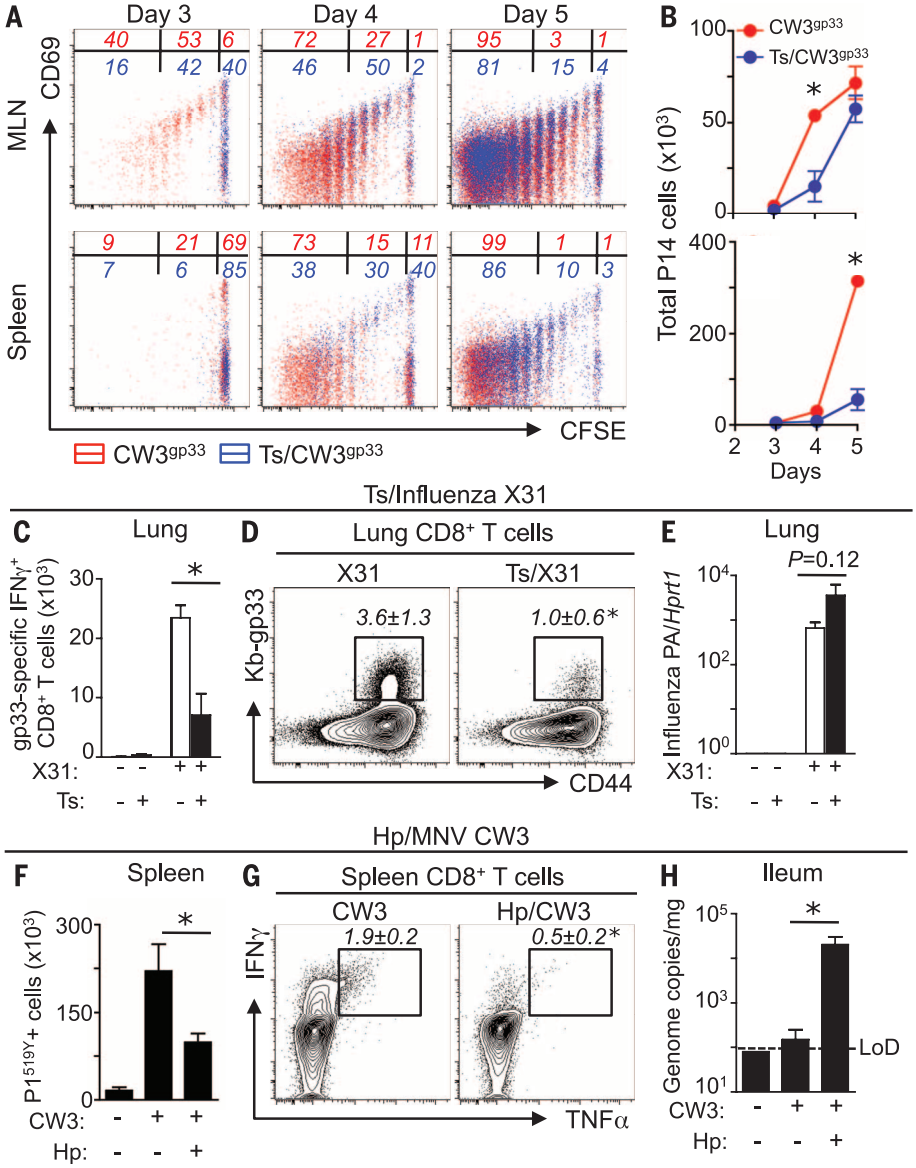

Fig. 2. Impaired virus-specific CD8$^+$ T cell activation and proliferation in the presence of helminth coinfection. (**A**) Carboxyfluorescein diacetate succinimidyl ester (CFSE) dilution and CD69 expression of adoptively transferred gp33-specific P14 CD8$^+$ T cells isolated from the MLNs and spleen of MNV CW3^{gp33} mono- and Ts/MNV CW3^{gp33}–coinfected mice. Red, monoinfected; blue, coinfected. Numbers in flow plots represent frequencies of cells in divisions 0, 1 to 5, or 6+ (right to left). (**B**) Quantification of total P14 cells in the MLNs (top row) and spleen (bottom row) in mono- and coinfected mice. (**C** to **E**) C57BL/6 mice were infected with 500 Ts larvae po. At day 12 post-Ts infection, mice were infected with 10^5 median tissue culture infectious dose influenza X31^{gp33} intranasally (in) and killed at day 7 post-X31 infection. (C) Lung lymphocytes from influenza X31^{gp33} monoinfected (X31) and coinfected (Ts/X31) mice were stimulated with gp33 peptide and assayed for production of IFN-γ. Total gp33-specific IFN-γ$^+$ CD8$^+$ T cells in the lung are shown. (D) Frequency of gp33-specific CD8$^+$ T cells in the lungs. Numbers in flow plots represent mean frequencies ± SEM of Kb-gp33 tetramer$^+$ cells within the CD8$^+$ lymphocyte gate of each group. (E) Quantification of influenza PA gene in lung tissue, normalized to *Hprt1*. (**F** to **H**) C57BL/6 mice were infected with 200 Hp larvae po. At day 12 post-Hp infection, mice were infected with 10^6 pfu MNV CW3 po and killed at day 7 post-CW3 infection. (F) Total splenic Kb-P1^{519Y} tetramer$^+$ CD8$^+$ T cells from CW3 monoinfected and Hp/CW3–coinfected mice. (G) Splenocytes were stimulated with P1^{519Y} peptide and assayed for production of IFN-γ and TNF-α. Numbers in flow plots represent mean frequencies ± SEM of dual-producing IFN-γ$^+$ TNF-α$^+$ cells within the CD8$^+$ CD44^{hi} lymphocyte gate of each group. (H) MNV genome copies in ileal tissue were quantified by RT-PCR. All data are representative of two independent experiments with a minimum of three to five mice per group. Bar graphs represent means ± SEM. Statistics compare monoinfected versus coinfected groups by using a two-way analysis of variance (ANOVA) with Bonferroni's post-testing [(B), (C), and (E)] or the Student's *t* test [(D) and (F) to (H)]. *$P < 0.05$.

it is critical to define the regulatory mechanisms by which helminth parasites can influence innate and adaptive immunity.

To test whether helminth infection elicits immunomodulation through direct effects on the mammalian immune system or via alterations in the microbiota, we developed a model of enteric coinfection using the helminth parasite *Trichinella spiralis* (Ts), which inhabits the small intestine for about 2 to 3 weeks before progressing to a persistent extraintestinal phase, and a murine norovirus (MNV CW3) that acutely infects the ileum. As expected, *Trichinella* infection induced type 2 immune responses (fig. S1). In the presence of the microbiota, *Trichinella*-MNV coinfection (fig. S2A) was associated with decreased frequencies and numbers of MNV-specific CD8$^+$ T cells within the small intestine, Peyer's patches, and spleen compared with monoinfected controls (Fig. 1, A and B, and fig. S2, B and C). Further, MNV-specific CD8$^+$ T cells isolated from helminth-coinfected mice exhibited diminished polyfunctional effector function as compared with monoinfected controls (Fig. 1C). Analysis of MNV-specific CD4$^+$ T cells using major histocompatibility complex II (MHCII) IA^b tetramers specific for an epitope (P1496) within the MNV capsid (table S1) identified that helminth-coinfected mice also had fewer antigen-specific CD4$^+$ T cells (fig. S2D) and impaired accumulation of virus-specific CD4$^+$ T cells expressing both interferon-γ (IFN-γ) and tumor necrosis factor–α (TNF-α) compared to monoinfected controls (Fig. 1D). Notably, the defective T cell responses were associated with elevated viral loads in intestinal tissue of *Trichinella*/MNV CW3–infected mice compared to monoinfected controls (Fig. 1E).

We generated a recombinant gp33-expressing strain of MNV CW3 (CW3^{gp33}) to track the activation and early proliferation of MNV-specific CD8$^+$ T cells in vivo. Adoptively transferred congenic gp33-specific P14 CD8$^+$ T cells accumulated and exhibited polyfunctional effector function in the intestine and spleen after MNV infection (fig. S3). Spatial and kinetic analysis of gp33-specific P14 CD8$^+$ T cell activation and proliferation revealed that helminth coinfection resulted in delayed virus-specific CD8$^+$ T cell proliferation and activation (Fig. 2A), as well as reduced or delayed accumulation of virus-specific T cells in the draining mesenteric lymph nodes (MLNs) and spleen (Fig. 2B). Similar to oral infection, systemic viral infection stimulated robust antiviral P14 CD8$^+$ T cell proliferation in monoinfected mice, which was dampened in helminth-coinfected mice (fig. S4), suggesting that helminth infection can impair systemic antiviral immune responses to MNV independent of inflammatory or tissue-repair processes operating in the intestine.

The immunomodulatory effects of *Trichinella* infection on antiviral immunity were long lived (fig. S5); able to influence established infection with MNV CR6, a related strain that persists in the colon of immune-competent mice (fig. S6); and evident in the lung after respiratory influenza infection (Fig. 2, C to E), indicating that helminth-elicited immunomodulation is operational at

extraintestinal tissues and can influence immunity to multiple viral pathogens. Further, the immunomodulatory effects of helminth infection on antiviral immunity were not restricted to *Trichinella* and were also evident after infection with *Heligmosomoides polygyrus bakeri* (Hp) (Fig. 2, F to H).

Despite ongoing clinical trials testing the potential efficacy of helminth immunotherapy to treat inflammatory diseases and the detrimental effects of helminth coinfection on protective immune responses to other human pathogens (*19*, *21*, *23*, *24*), the mechanisms underlying helminth-elicited immunomodulation remain poorly understood. Helminth infections can induce shifts in the composition of commensal bacterial communities, and these alterations have been proposed to play a role in modulating the host immune response (*13*–*18*). Further, commensal bacteria–derived signals can modulate lymphocyte responses to infection (*3*, *4*, *9*), including antiviral immunity (*25*–*27*). To test whether *Trichinella* infection altered the composition of the intestinal microbiota, we performed sequencing and phylogenetic analysis of bacterial 16*S* ribosomal RNA (rRNA) genes of small intestine and colon luminal contents. These analyses revealed alterations in commensal bacterial communities in both the small and the large intestine after *Trichinella* infection (Fig. 3, A to D). Notable changes included a reduction in the relative abundance of the *Turicibacteraceae* family and an increase in the relative abundance of *Lactobacillacaeae* in the small intestine (Fig. 3C) and increased colonic representation of *Clostridiales* (Fig. 3D).

To test whether these alterations contributed to helminth-induced immunomodulation, we compared the influence of helminth coinfection on antiviral immunity in the presence or absence of the microbiota using germ-free (GF) mice. Establishment of *Trichinella* in the intestine and peripheral tissues and induction of helminth-induced T helper 2 (T_H2) cell responses were similar in conventional (CNV) and GF mice (fig. S7). The diminished antiviral responses seen in helminth-coinfected mice were evident in both CNV and GF mice (Fig. 3, E to G). These data indicate that helminth-elicited immunomodulation of antiviral immunity can occur independently of changes in the microbiota and suggest that coevolution may have resulted in mechanisms that allow helminths to directly regulate host immune responses.

Helminth infection elicits the induction of type 2 cytokines and is associated with signal transducer and activator of transcription 6 (STAT6)–dependent alternative activation of macrophages (AAMacs), but these responses are not typically associated with protective antiviral immune responses. Therefore, we tested whether STAT6-dependent differentiation of AAMacs may underlie the dysregulated antiviral immune response in the context of helminth coinfection. Ex vivo analysis revealed a significant population expansion of macrophages ($CD11b^+$ $CD11c^-$ cells) in the MLNs of *Trichinella*-infected mice that was unaltered by MNV infection (Fig. 4A). Up-regulation of known AAMac-associated genes, including arginase-1 (*Arg1*), RELMα (*Retnla*), and Ym1 (*Chi3l3*), was detected in the ileum of wild-type (WT) but not STAT6- or

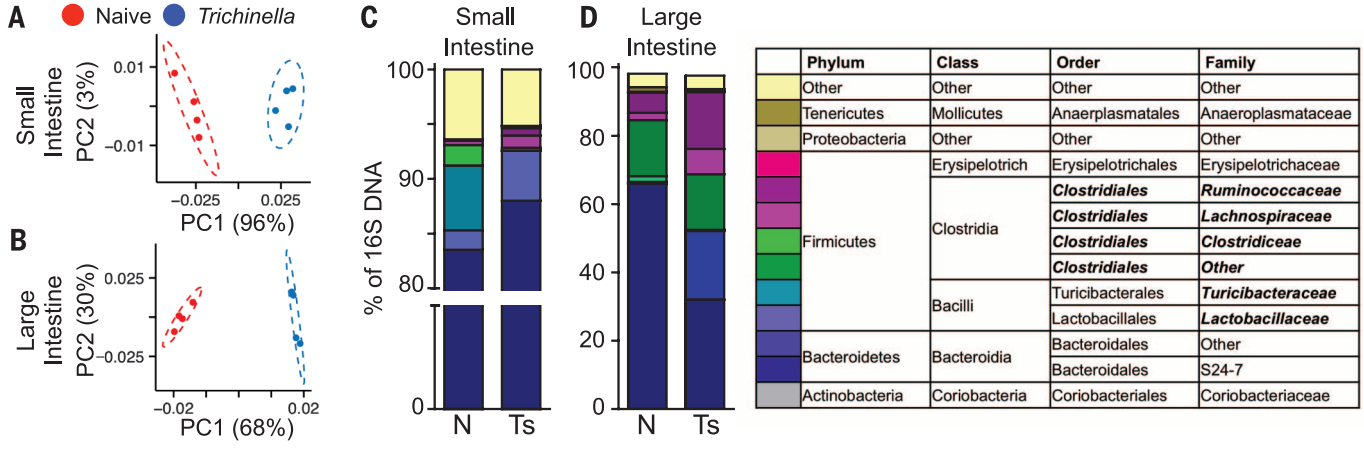

	Phylum	Class	Order	Family
	Other	Other	Other	Other
	Tenericutes	Mollicutes	Anaerplasmatales	Anaeroplasmataceae
	Proteobacteria	Other	Other	Other
	Firmicutes	Erysipelotrich	Erysipelotrichales	Erysipelotrichaceae
		Clostridia	***Clostridiales***	***Ruminococcaceae***
			Clostridiales	***Lachnospiraceae***
			Clostridiales	***Clostridiceae***
			Clostridiales	***Other***
		Bacilli	Turicibacterales	***Turicibacteraceae***
			Lactobacillales	***Lactobacillaceae***
	Bacteroidetes	Bacteroidia	Bacteroidales	Other
			Bacteroidales	S24-7
	Actinobacteria	Coriobacteria	Coriobacteriales	Coriobacteriaceae

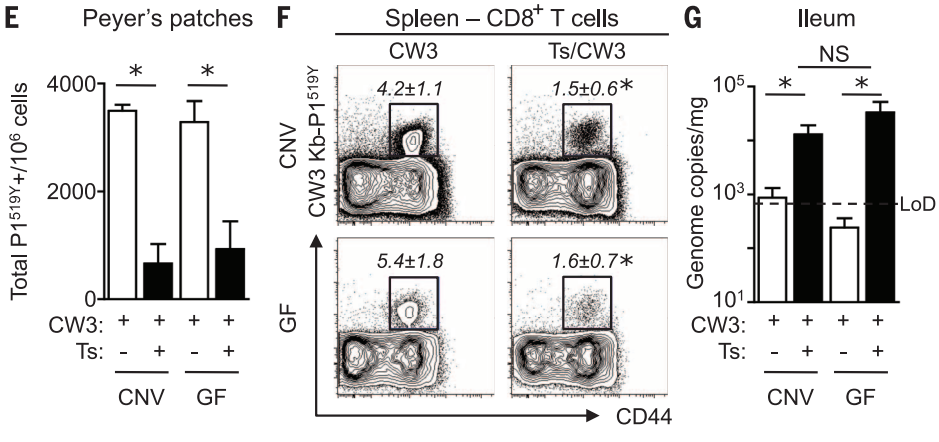

Fig. 3. Helminth-induced immunomodulation of antiviral immunity is independent of changes in the microbiota. (**A** to **D**) Luminal contents of the small and large intestines isolated from naïve or day 12 Ts-infected C57/BL6 mice were subjected to 16*S* sequencing by using Illumina MiSeq. Principal coordinate (PC) analysis of bacterial populations in the small intestine (A) and the large intestine (B) of naïve and Ts-infected mice. Axes represent weighted UniFrac distances between naïve and *Trichinella*-infected groups and are annotated, with the percentage of total variation explained. Statistical analyses were performed on groups of four mice, using PERMANOVA to test for differences in community composition according to weighted UniFrac centroid position. For (A), $P = 0.034$; (B), $P = 0.037$. Family-level phylogenetic analysis of bacterial sequences in the small (C) and the large (D) intestine of naïve and Ts-infected mice. In the legend on right, bold italicized taxa exhibited differences in relative abundance between naïve and Ts-infected mice. (**E** to **G**) Naïve and Ts-infected CNV or GF C57BL/6 mice were infected with MNV CW3 and killed at day 7 post-CW3. (E) MNV CW3 $P1^{519Y}$–specific $CD8^+$ T cells in the Peyer's patches of mono- and coinfected CNV and GF mice. (F) Frequency of MNV CW3 $P1^{519Y}$–specific $CD8^+$ T cells in the spleens of mono- and coinfected CNV and GF mice. Numbers in flow plots represent mean frequencies ± SEM of CW3 Kb-$P1^{519Y}$ $tetramer^+$ cells within the $CD8^+$ lymphocyte gate of each group. (G) MNV genome copies in ileal tissue were quantified by RT-PCR. Data in (E) to (G) are representative of three independent experiments with a minimum of three to five mice per group. Statistical analyses in (E) to (G) were performed by using two-way ANOVA with Bonferroni's post-testing. *$P < 0.05$. NS, not significant.

interleukin-4Rα (IL-4Rα)–deficient mice (Fig. 4B and fig. S8A), indicating that AAMac responses were evident in coinfected mice at the site of MNV CW3 infection. Critically, deletion of STAT6 was sufficient to restore MNV CW3^{gp33}–induced CD8$^+$ T cell proliferation (Fig. 4C), and mice lacking STAT6 or IL-4Rα exhibited reduced viral loads compared with coinfected WT controls after MNV infection (Fig. 4D and fig. S8B). Further, delivery of IL-4/anti-IL-4 complexes was sufficient to induce expression of AAMac-associated genes and impair antiviral immunity in vivo compared with control-treated mice (fig. S9). Collectively, these data suggest that AAMacs may limit the induction of host-protective antiviral immune responses in a type 2 cytokine- and STAT6-dependent manner.

Because MNV has tropism for macrophages (*28*), we tested the ability of bone marrow–derived macrophages (BM-Macs) to control viral replication. After recombinant IL-4 (rIL-4) treatment, BM-IL4 Macs undergo STAT6-dependent alternative activation, and BM-IL4 Macs infected with MNV CW3^{gp33} exhibited STAT6-dependent increases in viral burdens compared with control BM-Macs (fig. S10). Furthermore, although MNV CW3^{gp33}-infected control BM-Macs could elicit robust CD8$^+$ T cell proliferation in vitro, BM-IL4 Macs demonstrated STAT6-dependent inhibition of MNV-specific CD8$^+$ T cell proliferation (fig. S11A). To test whether AAMacs could modulate early antiviral immune responses in vivo, control BM-Macs or BM-IL4 Macs were adoptively transferred into mice along with MNV CW3^{gp33}. Mice receiving BM-IL4 Macs exhibited fewer antiviral CD8$^+$ T cells and increased viral burdens (fig. S11, B and C). Together, these data indicate that helminth-elicited STAT6-dependent induction of AAMacs can limit innate and adaptive immune responses to enteric viral infection.

AAMac effector molecules arginase-1, RELMα, and Ym1 have been implicated in regulating immunity and inflammation (*29*–*31*). However, antiviral CD8$^+$ T cell activation remained impaired in helminth-coinfected mice after inhibition of arginase-1 (fig. S12A) or deletion of RELMα (fig. S12B), indicating that these factors are dispensable for helminth-induced impairment of antiviral immunity. The chitinase-like molecule

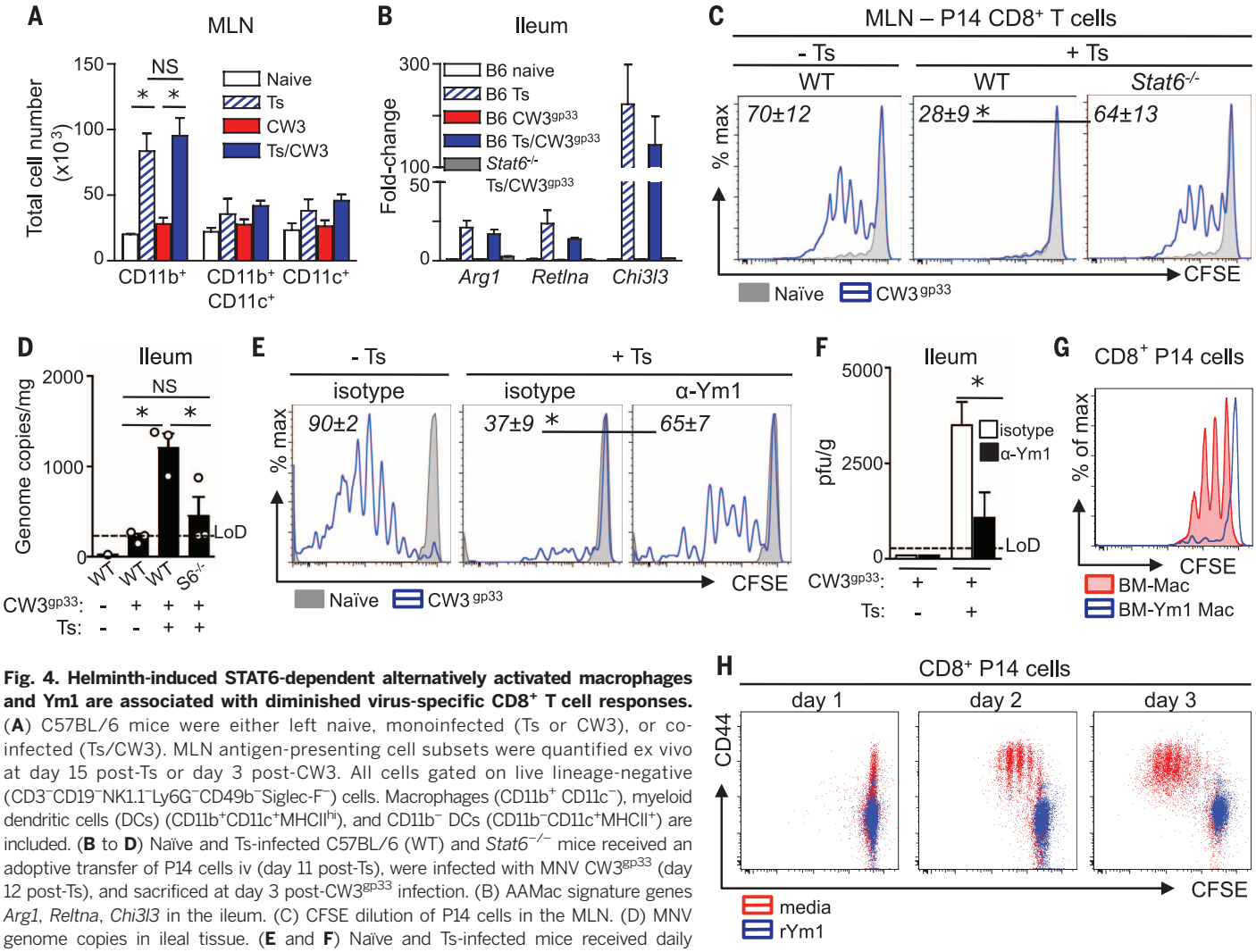

Fig. 4. Helminth-induced STAT6-dependent alternatively activated macrophages and Ym1 are associated with diminished virus-specific CD8$^+$ T cell responses. (**A**) C57BL/6 mice were either left naive, monoinfected (Ts or CW3), or coinfected (Ts/CW3). MLN antigen-presenting cell subsets were quantified ex vivo at day 15 post-Ts or day 3 post-CW3. All cells gated on live lineage-negative (CD3$^-$CD19$^-$NK1.1$^-$Ly6G$^-$CD49b$^-$Siglec-F$^-$) cells. Macrophages (CD11b$^+$ CD11c$^-$), myeloid dendritic cells (DCs) (CD11b$^+$CD11c$^+$MHCII^{hi}), and CD11b$^-$ DCs (CD11b$^-$CD11c$^+$MHCII$^+$) are included. (**B** to **D**) Naïve and Ts-infected C57BL/6 (WT) and *Stat6*$^{-/-}$ mice received an adoptive transfer of P14 cells iv (day 11 post-Ts), were infected with MNV CW3^{gp33} (day 12 post-Ts), and sacrificed at day 3 post-CW3^{gp33} infection. (B) AAMac signature genes *Arg1*, *Reltna*, *Chi3l3* in the ileum. (C) CFSE dilution of P14 cells in the MLN. (D) MNV genome copies in ileal tissue. (**E** and **F**) Naïve and Ts-infected mice received daily treatments of 300 μg of isotype mAb or anti-Ym1 starting at day 11 post-Ts infection and were MNV CW3^{gp33}–infected at day 12 post-Ts infection. (E) CFSE dilution of adoptively transferred P14 CD8$^+$ T cells in the MLN at day 3 post-CW3^{gp33} infection. (F) Viral load in the ileum as determined by plaque assay at day 7 post-CW3^{gp33} infection. (**G**) BM-Macs were infected with CW3^{gp33} and cultured with CFSE-labeled P14 CD8$^+$ T cells in the presence (blue trace) or absence (red fill) of rYm1 for 3 days. (**H**) Purified CFSE-labeled P14 CD8$^+$ T cells were stimulated with plate-bound αCD3 and soluble αCD28 in the presence (red) or absence (blue) of rYm1. Data in (A) to (F) are representative of one to three independent experiments with a minimum of three to five mice per group. Graphs represent means ± SEM. In (C) and (E), gray solid histogram, naïve mice; blue trace, CW3^{gp33}-infected. Numbers in flow plots represent mean frequencies ± SEM of CFSE-dividing P14 cells of each group. Data in (G) and (H) are representative of at least two independent experiments with technical replicates. Statistical analysis was performed by using two-way ANOVA with Bonferroni post-testing [(A) and (F)], Student's *t* test [(C) and (E)], or one-way ANOVA with Tukey's post-test (D). *P <0.05.

Ym1 is one of the most highly expressed AAMac effector molecules in multiple settings of acute and chronic type 2 cytokine-associated inflammation (*32*–*36*). Although Ym1 has been implicated in promoting chemoattraction and inflammation (*37*, *38*), the biological functions of this molecule are not well understood (*39*). To test whether Ym1 contributes to helminth-induced immunomodulation, virus-helminth–coinfected mice were treated with an isotype control monoclonal antibody (mAb) or a mAb against Ym1 (anti-YM1). Neutralization of Ym1 in coinfected animals significantly enhanced virus-specific $CD8^+$ T cell proliferation (Fig. 4E), the polyfunctional capacity of antiviral $CD8^+$ T cells, and the number of virus-specific $CD4^+$ T cells expressing effector cytokines (fig. S13). Anti-Ym1 treatment of coinfected mice was associated with enhanced control of viral replication (Fig. 4F). Further, although $CW3^{gp33}$-infected BM-Macs stimulated robust P14 $CD8^+$ T cell proliferation, this was inhibited by addition of recombinant Ym1 (rYm1) (Fig. 4G). rYM1 was also sufficient to inhibit T cell receptor–driven activation and proliferation of purified $CD8^+$ T cells (Fig. 4H). Taken together, these findings reveal a role for helminth-induced AAMacs and Ym1 in immunomodulation of protective immune responses to concomitant viral infection.

These data identify that helminth coinfection can inhibit antiviral immunity via a pathway of innate immunomodulation. This was independent of changes in the microbiota but associated with induction of potent AAMac responses and Ym1-dependent inhibition of antiviral T cell responses (fig. S14). Therefore, although helminth parasites and commensal bacteria colonize the same niche within the intestine, coevolution of helminths with their mammalian hosts may have resulted in mechanisms that allow direct regulation of the host innate immune system and antiviral immunity independently of changes in the microbiota. These findings, coupled with a report by Reese *et al.* (*40*) identifying a critical role for helminth-induced IL-4/IL-13 and STAT6 activity in reactivation of latent γ-herpesvirus infection in macrophages, indicate a conserved mechanism of innate immunomodulation in the context of virus-helminth coinfection. The identification of an immunomodulatory role for the AAMac-Ym1 pathway could have implications for the development of helminth-based therapies for multiple chronic inflammatory diseases as well as improved vaccination strategies in helminth-infected individuals.

REFERENCES AND NOTES

1. A. J. Macpherson, N. L. Harris, *Nat. Rev. Immunol.* **4**, 478–485 (2004).
2. L. V. Hooper, D. R. Littman, A. J. Macpherson, *Science* **336**, 1268–1273 (2012).
3. A. Benson, R. Pifer, C. L. Behrendt, L. V. Hooper, F. Yarovinsky, *Cell Host Microbe* **6**, 187–196 (2009).
4. J. A. Hall *et al.*, *Immunity* **29**, 637–649 (2008).
5. S. Vaishnava, C. L. Behrendt, A. S. Ismail, L. Eckmann, L. V. Hooper, *Proc. Natl. Acad. Sci. U.S.A.* **105**, 20858–20863 (2008).
6. K. Atarashi *et al.*, *Science* **331**, 337–341 (2011).
7. K. S. Hayes *et al.*, *Science* **328**, 1391–1394 (2010).
8. M. Raetz *et al.*, *Nat. Immunol.* **14**, 136–142 (2013).
9. I. I. Ivanov *et al.*, *Cell* **139**, 485–498 (2009).
10. D. R. Littman, E. G. Pamer, *Cell Host Microbe* **10**, 311–323 (2011).
11. J. E. Allen, R. M. Maizels, *Nat. Rev. Immunol.* **11**, 375–388 (2011).
12. D. E. Elliott, J. V. Weinstock, *Ann. N. Y. Acad. Sci.* **1247**, 83–96 (2012).
13. S. Rausch *et al.*, *PLOS ONE* **8**, e74026 (2013).
14. S. T. Walk, A. M. Blum, S. A. Ewing, J. V. Weinstock, V. B. Young, *Inflamm. Bowel Dis.* **16**, 1841–1849 (2010).
15. M. J. Broadhurst *et al.*, *PLOS Pathog.* **8**, e1003000 (2012).
16. R. W. Li *et al.*., *Infect. Immun.* **80**, 2150–2157 (2012).
17. A. J. Bancroft, K. S. Hayes, R. K. Grencis, *Trends Parasitol.* **28**, 93–98 (2012).
18. J. M. Leung, P. Loke, *Int. J. Parasitol.* **43**, 253–257 (2013).
19. E. Stelekati, E. J. Wherry, *Cell Host Microbe* **12**, 458–469 (2012).
20. P. Salgame, G. S. Yap, W. C. Gause, *Nat. Immunol.* **14**, 1118–1126 (2013).
21. S. Metenou, S. Babu, T. B. Nutman, *Curr Opin HIV AIDS* **7**, 231–238 (2012).
22. J. A. Potian *et al.*, *J. Exp. Med.* **208**, 1863–1874 (2011).
23. M. J. Wolff, M. J. Broadhurst, P. Loke, *Trends Parasitol.* **28**, 187–194 (2012).
24. H. J. McSorley, R. M. Maizels, *Clin. Microbiol. Rev.* **25**, 585–608 (2012).
25. T. Ichinohe *et al.*, *Proc. Natl. Acad. Sci. U.S.A.* **108**, 5354–5359 (2011).
26. M. C. Abt *et al.*, *Immunity* **37**, 158–170 (2012).
27. S. C. Ganal *et al.*, *Immunity* **37**, 171–186 (2012).
28. C. E. Wobus *et al.*, *PLOS Biol.* **2**, e432 (2004).
29. J. T. Pesce *et al.*, *PLOS Pathog.* **5**, e1000371 (2009).
30. J. T. Pesce *et al.*, *PLOS Pathog.* **5**, e1000393 (2009).
31. M. G. Nair *et al.*, *J. Exp. Med.* **206**, 937–952 (2009).
32. P. Loke *et al.*, *BMC Immunol.* **3**, 7 (2002).
33. J. Zhao *et al.*, *Parasitol. Res.* **112**, 2689–2695 (2013).
34. M. G. Nair *et al.*, *Infect. Immun.* **73**, 385–394 (2005).
35. A. Q. Ford *et al.*, *BMC Immunol.* **13**, 6 (2012).
36. N. C. Chang *et al.*, *J. Biol. Chem.* **276**, 17497–17506 (2001).
37. M. Owhashi, H. Arita, N. Hayai, *J. Biol. Chem.* **275**, 1279–1286 (2000).
38. M. Arora *et al.*, *Proc. Natl. Acad. Sci. U.S.A.* **103**, 7777–7782 (2006).
39. T. E. Sutherland, R. M. Maizels, J. E. Allen, *Clin. Exp. Allergy* **39**, 943–955 (2009).
40. T. A. Reese *et al.*, *Science* **345**, 573 (2014).

ACKNOWLEDGMENTS

We thank members of the Artis laboratory for discussions and critical reading of the manuscript; F. Finkelman for providing anti–IL-4 clone 1D11.2; the NIH Tetramer Core Facility (contract HHSN272201300006C) for providing MHCII IA^b tetramers; the University of Pennsylvania Matthew J. Ryan Veterinary Hospital Pathology Lab, the NIH/National Institute of Diabetes and Digestive and Kidney Diseases Center for Molecular Studies in Digestive and Liver Diseases (P30-DK050306), and its core facilities (Molecular Pathology and Imaging, Molecular Biology, Cell Culture, and Transgenic and Chimeric Mouse); the Penn Center for AIDS Research (P30-AI045008) for assistance and support; and the Abramson Cancer Center Flow Cytometry and Cell Sorting Resource Laboratory for technical advice and support. The ACC Flow Cytometry and Cell Sorting Shared Resource is partially supported by a National Cancer Institute Comprehensive Cancer Center Support grant (2-P30 CA016520). The data tabulated in this paper are reported in the main paper and in the supplementary materials. Illumina MiSeq data can be found in the National Center for Biotechnology Information Sequence Read Archive with accession number SRP043964. Research in the Artis lab is supported by the NIH (AI061570, AI074878, AI087990, AI095466, AI095608, AI097333, AI106697, and AI102942 to D.A.; T32-AI007532 to L.A.M.; and F32-AI085828 to M.C.S.), the Crohn's and Colitis Foundation of America (D.A. and M.R.H.), the Burroughs Wellcome Fund Investigator in Pathogenesis of Infectious Disease Award (D.A.), and the Edmond J. Safra Foundation/Cancer Research Institute Irvington Fellowship (L.C.O.). E.J.W. and V.T.T. are supported by NIH grants AI083022, AI082630, and K08-DK097301. T.E.S. and J.E.A. were supported by the Medical Research Council UK (MR/J001929/1). T.J.N. was supported by NIH training grant 5T32A100716334 and postdoctoral fellowships from the Cancer Research Institute and American Cancer Society. H.W.V. was supported by grant R01 AI 084887, the Crohn's and Colitis Genetics Initiative grant 274415, and the Broad Foundation grant IBD-0357. Washington University and H.W.V. receive income based on licenses for MNV technology. The authors declare no other potential conflicts of interest.

SUPPLEMENTARY MATERIALS

www.sciencemag.org/content/345/6196/578/suppl/DC1
Materials and Methods
Supplementary Text
Figs. S1 to S14
Table S1
References (*41*–*57*)

4 June 2014; accepted 8 July 2014
Published online 17 July 2014;
10.1126/science.1256942